

## COLLAPSAR UNCORKING AND JET ERUPTION IN GAMMA-RAY BURSTS

E. WAXMAN<sup>1</sup> AND P. MÉSZÁROS<sup>2</sup>

Received 2002 June 22; accepted 2002 October 14

### ABSTRACT

We show that the collapsar model of gamma-ray bursts results in a series of successive shocks and rarefaction waves propagating in the “cork” of stellar material being pushed ahead of the jet, as it emerges from the massive stellar progenitor. Our results are derived from analytical calculations assuming a hot, ultrarelativistic one-dimensional flow with an initial Lorentz factor  $\Gamma_j \sim 100$ . The shocks result in a series of characteristic, increasingly shorter and harder thermal X-ray pulses, as well as a nonthermal  $\gamma$ -ray pulse, which precede the usual nonthermal MeV  $\gamma$ -rays. We consider jets escaping from both compact (CO or He dwarf) and blue supergiant stellar progenitors. The period, fluence, and hardness of the pulses serves as a diagnostic for the size and density of the outer envelope of the progenitor star.

*Subject headings:* gamma rays: bursts — gamma rays: theory — supernovae: general — X-rays: bursts

*On-line material:* color figures

### 1. INTRODUCTION

The nonthermal radiation from shocks in a relativistic fireball jet after emerging from a collapsing massive stellar system (collapsar) is the leading theoretical explanation for the family of “long” gamma-ray bursts (GRB) with  $\gamma$ -ray durations longer than about  $t_b \sim 10$  s (Woosley 1993; Paczyński 1998; see Mészáros 2002 for a review). The jet is thought to arise from a brief accretion episode of a rotating debris torus around a central black hole formed as the stellar core collapses. The nature and history of the massive star, however, is so far largely a matter of hypothesis and calculation, and alternative stellar progenitor systems are conceivable, both for the long and especially for the shorter bursts.

The duration of the TeV neutrino burst expected from shocks in the jet before it emerges is a possible diagnostic for the pre-emergence jet history and for the dimensions or column density of the progenitor stellar system (Mészáros & Waxman 2001). Previous analytical work on shock and jet emergence has been done by Matzner & McKee (1999), Mészáros & Rees (2001), and Matzner (2002), and numerical calculations of relativistic jets have been done by Martiet al. (1997), Aloy et al. (2000), and Zhang, Woosley, & McFadyen (2002). Here we concentrate on possible photon signatures of the jet as it emerges, which precedes the usual gamma-ray emission and the subsequent longer wavelength afterglow. This has been considered by Ramirez-Ruiz, McFadyen, & Lazzati (2002), who infer an X-ray precursor to the burst from the portion of the stellar envelope shocked by the jet. Here we investigate in some detail, using analytical one-dimensional methods in the ultrarelativistic limit, the jet emergence process and the shock heating and expansion of the plug of stellar material propelled by it, resembling an ejected cork.

In the initial stage of ejection the cork is optically very thick to scattering, and it experiences successive shocks and rarefactions as the optical depth decreases during its overall

expansion. This leads to an X-ray photon precursor to the usual GRB emission, consisting of a pattern with an initial rise and decay followed by a brighter and harder peak, possibly repeated a few times with decreasing period. The characteristic timescale of the initial decay and the ratio of its amplitude to that of the peak differ substantially depending on the density and extent of the envelope, thus providing a potential diagnostic for the preburst stellar configuration. These precursor patterns should be detectable with instruments to be flown in the next few years.

### 2. JET PROPAGATION

We assume a jet with isotropic equivalent luminosity  $L_{\text{iso}} \gtrsim 10^{52} L_{52}$  ergs  $s^{-1}$  and Lorentz factor  $\Gamma_j \sim 10^2$ . As the jet advances through the star, it drives forward a bow shock into the star. The jet is capped by a “cork” composed of a termination shock advancing into the star, and a reverse shock moving back into the jet, where the tenuous and highly relativistic jet gas is suddenly decelerated and compressed. Both the shocked jet plasma and the shocked stellar plasma advance inside the star with a jet head Lorentz factor  $\Gamma_h \ll \Gamma_j$ , corresponding to a velocity  $\beta_h$ . Figure 1 presents a schematic description of the multiple shock structure. In the rest frame of the shocked, decelerated plasma, the fast jet moves with a Lorentz factor  $\sim \Gamma_j/2\Gamma_h$ . During propagation in the He core, the high density ahead of the jet,  $\rho \sim 1$  g  $cm^{-3}$ , implies deceleration of the jet plasma to a subrelativistic velocity. However, beyond the C/O or He core edge at  $r \gtrsim 10^{10}$ – $10^{11}$  cm, there is a sharp drop in the density, e.g., the density of an H envelope, if present, is typically  $\rho \sim 10^{-5}$ – $10^{-7}$  g  $cm^{-3}$ , and the jet can accelerate to relativistic velocity. We have used Matzner & McKee’s parametrization of the density drop near the edge of the star,  $r = R_*$ ,

$$\rho = \rho_* \left( \frac{R_*}{r} - 1 \right)^n, \quad (1)$$

where  $n = 3$  (3/2) for radiative (convective) envelope. Equation (1) holds for a polytropic plasma at radii beyond which the envelope contribution to the gravitational potential is small. We consider three progenitor examples: (1) the

<sup>1</sup> Weizmann Institute of Science, Rehovot 76100, Israel.

<sup>2</sup> Pennsylvania State University, University Park, PA 16803.

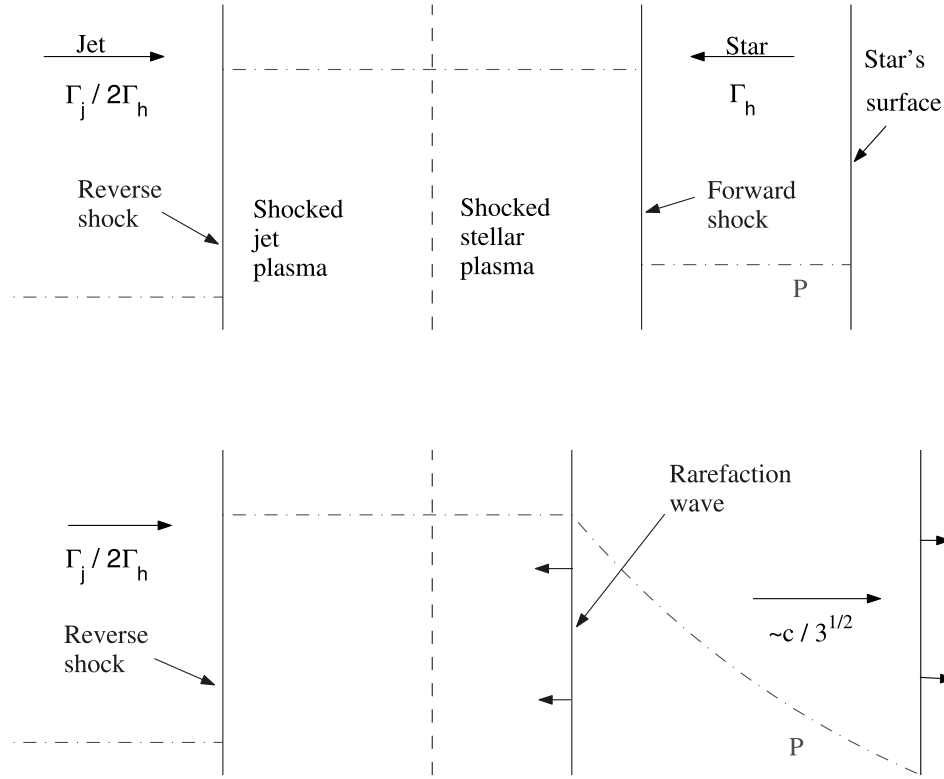


FIG. 1.—*Top*: Schematic description of the double shock structure at the head of the jet, as seen in the frame where the shocked plasma is at rest, during jet propagation within the star. The dot-dashed line shows the pressure distribution. *Bottom*: Schematic description of the flow after forward-shock break-out. A rarefaction wave propagates backward into the shocked plasma, and the plasma ahead of this wave expands with velocity comparable to the speed of sound. When the rarefaction wave reaches the backward shock, a new double-shock structure similar to that shown on the top panel is formed, propagating through the expanding shocked plasma. [See the electronic edition of the Journal for a color version of this figure.]

edge of the C/O progenitor model of SN 1998bw (Woosley, Eastman, & Schmidt 1999), approximately described by  $\rho_* = 5 \times 10^2 \text{ g cm}^{-3}$ ,  $R_* = 10^{10} \text{ cm}$ , and  $n = 3$ ; (2) the outer part of the He mantle of the presupernova model, evolved by Woosley, Langer, & Weaver (1993) from a  $35 M_\odot$  main-sequence star, approximately described by equation (1) with  $\rho_* = 2 \text{ g cm}^{-3}$ ,  $R_* = 10^{11} \text{ cm}$ , and  $n = 3$ ; and (3) the envelope of the blue supergiant (BSG) progenitor models of SN 1987A (Shigeyama & Nomoto 1990; Arnett 1991), approximately described by  $\rho_* = 3 \times 10^{-5} \text{ g cm}^{-3}$ ,  $R_* = 3 \times 10^{12} \text{ cm}$ , and  $n = 3$ . Taking in equation (1) a radius  $r \simeq 0.9R_*$ , we take as approximate reference quantities the values  $\rho \sim (1, 10^{-3}, 10^{-7}) \text{ g cm}^{-3}$  at  $r \sim (10^{10}, 10^{11}, 10^{12.5}) \text{ cm}$  for a C/O core, He core, and BSG star H envelope, respectively.

The pressure behind the forward shock is given for  $\Gamma_h \gg 1$  by  $P_h = \frac{4}{3}\Gamma_h^2 \rho c^2$ , and for  $\beta_h \ll 1$  by  $P_h = [(\bar{\gamma} + 1)/2]\rho\beta_h^2 c^2$ , where  $\bar{\gamma} = \frac{4}{3}$  is the adiabatic index of the plasma (radiation dominated). The  $\Gamma_h$  is given by equating  $P_h$  with the pressure behind the reverse shock,  $P_r = \frac{4}{3}(\Gamma_j/2\Gamma_h)^2 n_j m_p c^2$  for  $\Gamma_h \gg 1$  and  $P_r = \frac{4}{3}\Gamma_j^2 n_j m_p c^2$  for  $\beta_h \ll 1$ , where the jet proper proton density  $n_j = L_{\text{iso}}/(4\pi r^2 \Gamma_j^2 m_p c^3)$ . (For a discussion of relativistic flows and shock jump conditions, see, e.g., Begelman, Blandford, & Rees 1984). The extreme relativistic limit gives (Mészáros & Waxman 2001)

$$\Gamma_h \sim \begin{cases} 1.6L_{52}^{1/4}/r_{12.5}^{1/2}\rho_{-7}^{1/4} & \text{H} , \\ 0.9L_{52}^{1/4}/r_{11}^{1/2}\rho_{-3}^{1/4} & \text{He} , \end{cases} \quad (2)$$

for the H envelope of a BSG (H) or a He star, while the non-relativistic limit gives

$$\beta_h \sim \begin{cases} 1.6L_{52}^{1/2}/r_{11}\rho_{-3}^{1/2} & \text{He} , \\ 0.6L_{52}^{1/2}/r_{10}\rho_0^{1/2} & \text{CO} , \end{cases} \quad (3)$$

for the He or CO cores, where more exactly  $\beta_h \leq 1$  and  $\Gamma_h \geq 1$  would hold;  $L_{\text{iso}} = 10^{52} L_{52} \text{ ergs s}^{-1}$  is the jet isotropic equivalent luminosity,  $r = 10^x r_x \text{ cm}$  is the shock radius, and  $\rho = 10^x \rho_x \text{ g cm}^{-3}$  is the corresponding density at that radius. These values are for the main part of the cork, including the shocked jet and the bulk of the shocked stellar material. Thus, for  $r \sim 0.9R_*$  in all cases the jet head velocity is at least marginally relativistic, and this approximation gets better as  $r \rightarrow R_*$ . This implies that, even though the jet injected at the base of the jet is assumed to be ultrarelativistic,  $\Gamma_j = 10^2 \Gamma_2 \gg 1$ , the jet head advances subrelativistically for most of its initial crossing of the stellar interior. This is due to the initial inertia of the dense stellar material, which needs to be pushed ahead and aside (e.g., Mészáros & Rees 2001 for an analytical discussion). A similar relativistic injection and subrelativistic jet head advance occurs in active galactic nucleus (AGN) jets encountering the intergalactic medium, e.g., Begelman et al. (1984). The jet crossing time out to the He (or CO) core edge is of the order of  $t_{\text{core}} \lesssim 30r_{11} \text{ s}$  for a jet that has reached  $v_h \sim c$  near the core edge, suggesting that compact ( $r \lesssim 10^{11} \text{ cm}$ ) stars such as He stars or pre-WR stars are likely GRB progenitors (see also MacFadyen, Woosley, & Heger 2001; Matzner 2002).

However, if there is an H envelope beyond the C/O/He core, where the density drops steeply by  $10^{-5}$  to  $10^{-7}$ , momentum conservation indicates that  $\Gamma_h$  for the entire cork (eq. [2]) can become significantly larger at radii just beyond  $r_{\text{core}} = 10^{11} R_{11}$  cm. This jump in  $\Gamma_h$  is absent in Matzner's (2002) treatment, which approximates with an unvarying  $\rho \propto r^{-2}$  dependence the entire density profile on either side and across the He-H transition. A density drop steeper than  $r^{-2}$  is, however, expected at this core-envelope transition for radiative envelopes (eq. [1]), and is a distinctive feature of the numerical precollapse models employed above. Using equation (2) for the Lorentz factor of the entire cork in an H envelope, the additional crossing time can be much, much smaller than the core crossing time already incurred,  $t_H \sim r_H/2c\Gamma_h^2 \ll t_{\text{core}}$  (Mészáros & Rees 2001), as long as the envelope is not too extended,  $r_H \lesssim \text{few} \times 10^{12}$  cm, e.g., for blue supergiants (BSG). This is independent of whether a small fraction of the outermost cork mass is accelerated along the density gradient to larger Lorentz factors (Matzner & McKee 1999), as discussed in the next section. The only other restriction besides the envelope size is that the envelope mass should be smaller than that inside the stellar core, which is generally true for BSGs. Thus, the jet "powering" time,  $t_j$ , needed to produce an emerging jet (and hence a successful GRB) is limited mainly by the core crossing time  $t_{\text{core}} \sim 30$  s, which is similar both for envelope-stripped CO or He stars and for stars as extended as blue supergiants with H envelopes of  $r_H \lesssim \text{few} \times 10^{12}$  cm.

The cork is composed of shocked jet and stellar plasma. The comoving width of the shocked jet plasma is  $\Delta_j = 0.2\theta r$  (Mészáros & Waxman 2001), where  $\theta$  is the asymptotic jet opening angle. The comoving width of the shocked stellar plasma is obtained by balancing the mass flux across the bow shock,  $\approx \pi(\theta r^2)(\beta_h c + v_s')(\Gamma_h \rho)$ , where  $v_s'$  is the shock velocity in the cork frame, with the tangential flux of particles leaving the cylinder of (cork frame) height  $\Delta_s$  and radius  $\theta r$  of shocked plasma,  $\approx 2\pi\theta r \Delta_s c_s \rho'$ , where  $c_s$  and  $\rho'$  are the postshock speed of sound and density, respectively. Using  $c_s = c/\sqrt{3}$  and  $\rho' = 4\Gamma_h \rho$  for the relativistic ( $\Gamma_h \gg 1$ ) case, which from now on we take as approximately valid for all cases considered, we obtain  $\Delta_0 \simeq 0.2\theta r$ . The Thomson optical depth of the shocked stellar plasma is thus

$$\tau_{T,s} \simeq \begin{cases} 1.5 \times 10^4 \theta_{-1} L_{52}^{1/4} r_{12.5}^{1/2} \rho_{-7}^{3/4}, & \text{H}, \\ 2.7 \times 10^6 \theta_{-1} L_{52}^{1/4} r_{11}^{1/2} \rho_{-3}^{3/4}, & \text{He}, \\ 1.5 \times 10^8 \theta_{-1} L_{52}^{1/4} r_{10}^{1/2} \rho_0^{3/4}, & \text{CO}. \end{cases} \quad (4)$$

Here,  $\theta = 0.1\theta_{-1}$ . The cork temperature is

$$T_r \simeq \begin{cases} 1.6 L_{52}^{1/8} r_{12.5}^{-1/4} \rho_{-7}^{1/8} \text{ keV}, & \text{H}, \\ 12 L_{52}^{1/8} r_{11}^{-1/4} \rho_{-3}^{1/8} \text{ keV}, & \text{He}, \\ 50 L_{52}^{1/8} r_{10}^{-1/4} \rho_0^{1/8} \text{ keV}, & \text{CO}. \end{cases} \quad (5)$$

The corresponding (cork frame) energy carried by the cork is thus

$$E_0 \simeq \begin{cases} 3.9 \times 10^{48} L_{52}^{3/4} \theta_{-1}^3 r_{12.5}^2 \text{ ergs}, & \text{H}, \\ 4.3 \times 10^{45} L_{52}^{3/4} \theta_{-1}^3 r_{11}^2 \text{ ergs}, & \text{He}, \\ 4.3 \times 10^{43} L_{52}^{3/4} \theta_{-1}^3 r_{10}^2 \text{ ergs}, & \text{CO}. \end{cases} \quad (6)$$

### 3. JET EMERGENCE: X-RAY PRECURSOR

#### 3.1. Dynamics

As the forward shock approaches the stellar edge it accelerates to relativistic velocity. At some finite depth  $d = R - r$  it becomes causally disconnected from the backward shock. This occurs at the point where during a sound crossing time of the cork,  $\delta t \approx \Gamma_h 0.4\theta r/c_s$ , the forward shock accelerates significantly. Since  $\Gamma_h \propto \rho^{-1/4}$  (as long as the forward shock is causally connected to the backward one), the fractional change in the shock Lorentz factor is  $\delta\Gamma/\Gamma \approx \delta\rho/4\rho = c\delta t d \ln \rho/dr \approx 0.4\Gamma_h(c/c_s)\theta r(n/4)/(R_* - r)$ . Thus, the forward shock becomes disconnected at  $d \equiv R_* - r \approx \Gamma_h(d)\theta r$ , where  $\delta\Gamma/\Gamma \approx 1$  [here  $\Gamma_h(d)$  is the main cork Lorentz factor at depth  $d$ ]. Denoting by  $\Gamma_*$  the value of  $\Gamma_h$  given by equation (2) for  $r = R_*/2$ , assuming the density profile of equation (1), we find  $d/R_* \approx (\Gamma_*\theta)^{4/(n+4)}$  and  $\Gamma_h(d) \approx \Gamma_*^{4/(n+4)} \theta^{-n/(n+4)}$ . Assuming  $\theta \approx 1/15$ , the value inferred by Frail et al. (2001), we find that the cork is mildly relativistic at the onset of "runaway" for all the progenitors (He, BSG, C/O) considered above. The dependence of  $\Gamma_h(d)$  on  $\theta$  is not very strong,  $\Gamma_h(d) \propto \rho(d)^{-1/4} \propto (d/R)^{-n/4} \propto \theta^{-n/(n+4)}$ . The stellar densities at "runaway" onset are  $\sim 1$ ,  $\sim 10^{-3}$ , and  $\sim 10^{-7}$  g cm $^{-3}$  for the C/O, He, and BSG progenitors, respectively.

As the forward shock reaches depth  $d$ , it accelerates and breaks through the stellar edge before the backward shock reacts to the rapid acceleration. During jet propagation in the envelope, the shocked cork plasma is pushed sideways, away from the jet path, on a timescale  $\Gamma_h \theta r/c_s$ . Since the forward shock runaway, from depth  $d$  outward, takes place on a similar timescale, we can assume that the cork is "frozen" during this time. At break-out we will therefore have a cork of thickness  $0.4\theta R_*$ , with density, temperature, and velocity given by the equations of § 2 with  $r = R_*$  and density  $\rho(R_* - d)$ . Ahead of this cork, there will be a faster moving shell of plasma, accelerated during shock runaway (similar to that considered in spherical supernova shocks by Matzner & McKee 1999). The column density of the faster plasma is smaller than that of the cork by a factor of  $\approx 1/(n+1)$ .

During the shock runaway, the pressure behind the forward shock is smaller than that behind the backward shock (since the two are causally disconnected). The forward-shock Lorentz factor is therefore smaller than that given by equation (2), using the density ahead of the forward shock:  $\Gamma(x) \approx (x/d)^{-n/4}$ , where  $x$  is the depth. The optical depth at depth  $x$  is  $\tau(x) \approx [\tau_{T,s}/(n+1)](x/d)^{n+1}$ , where  $\tau_{T,s}$  is the cork optical depth, implying  $\Gamma(x) \approx [\tau_{T,s}/(n+1)\tau(x)]^{n/4(n+1)}$ . Since the shocks are radiation dominated, the maximum Lorentz factor to which plasma is accelerated is smaller than that given by this expression for  $\tau(x) = 1$ . Using equation (4), we find that the maximum Lorentz factor is of the order of 10 for all progenitor types mentioned above.

Whether or not a fast,  $\Gamma \sim 10$  shell is ejected ahead of the cork is unclear. As the forward shock accelerates and becomes disconnected from the driving jet "piston," it is likely to become unstable (as commonly found in the nonrelativistic case, e.g., Sari, Waxman, & Shvarts 2000). Moreover, if the progenitor plasma is magnetized, the magnetic field may also prevent large  $\Gamma$  gradients. We therefore consider in the following subsection X-ray emission from the slower, main cork plasma. We briefly comment here on how a fast shell ahead of the cork may affect this X-ray emission.

Photons emitted by the cork would overtake the fast shell, spend some time diffusing through it, and then escape. Let us first consider the time delay introduced to photon arrival times seen by a distant observer. We show below that the fast shell does not change its radius significantly during the photon diffusion through it. The time delay can therefore be decomposed into two separate contributions: a geometric time delay due to a change in the photon propagation direction, which is assumed to take place instantaneously at the shell overtaking radius, and a diffusion time delay due to the fact that the effective velocity of the photon during the time it spends in the shell is smaller than  $c$  [by  $c/2\Gamma(x)^2$ ].

As shown below, the timescale of photon emission from the cork is  $t_0 \sim \theta R_*/c$ . Photons emitted radially from the cork at time  $t$  following break-out will overtake a fast shell with  $\Gamma(x)$  at time  $t_1 \sim 2\Gamma(x)^2 t$ . For  $t \gtrsim t_0$ , a fast shell with  $\Gamma(x) > \theta^{-1/2}$  expands significantly by  $t_1$ ,  $ct_1/R_* \sim \Gamma(x)^2 \theta$ . In this case, the spread in overtaking times between photons emitted radially and nonradially from the cork,  $\sim \theta^2 R_*/c$ , is small compared to  $t_0$ , and we can consider geometric time delay of radial photons only. For an observer along the jet axis, the geometric time delay between two photons emitted at time  $t$  and scattered toward the observer from different points in the fast shell, one from a point along the line of sight and the other from the edge of the shell, propagating at angle  $\theta$  with respect to the line of sight (we have shown above that  $\Gamma(x) < 10 \lesssim 1/\theta$ , so that such scattering is possible), is  $\approx 0.5\theta^2 t_1 \approx [\Gamma(x)\theta]^2 t$ . Since  $\Gamma(x)\theta < 1$ , the time spread introduced by this geometric time delay would not affect significantly the shape of the pulse emitted by the cork plasma.

Let us now consider the diffusion time delay. For  $t \gtrsim t_0$ , the optical depth of the shell at  $t_1$  is  $\tau_1(x) \approx \tau(x)(ct_1/R_*)^{-2}$ . Since the proper thickness of the fast shell is  $x/\Gamma(x)$  (due to the shock compression), the photon diffusion time through the shell is  $\approx \tau_1 x/\Gamma(x)c$  in the shell frame, corresponding to  $\delta t_{\text{diff}} \approx \tau_1 x/c$  in the star frame. The delay in photon propagation (compared to free propagation) is  $\delta t_{\text{prop}} \approx \delta t_{\text{diff}}/2\Gamma(x)^2$ . For  $t \gtrsim t_0$  we thus find  $\delta t_{\text{prop}}/t_0 \sim [\tau_{T,s}/(n+1)\theta^2] (t/t_0)^{-2} \Gamma(x)^{-2(5n+4)/n}$ . For  $n=3$ , the diffusion time delay is small, compared to  $t_0$ , for  $\Gamma(x) > [\tau_{T,s}/(n+1)\theta^2]^{3/38}$ . Using equation (4), we conclude that this time delay is small for  $\Gamma(x) > a$  few. The fractional change in the shell radius during photon diffusion,  $\sim \delta t_{\text{diff}}/2\Gamma(x)^2 t \approx \delta t_{\text{prop}}/t < \delta t_{\text{prop}}/t_0$ , is also small, justifying our assumption that the shell radius is approximately constant over a photon diffusion time.

The arguments given above demonstrate that the fast shell would not significantly affect the pulse shape. Let us now consider its effect on the photon spectrum. The comoving postshock temperature decreases toward the stellar edge,  $T(x)^4 \propto \Gamma(x)^2 \rho(x) \propto \rho(x)^{1/2}$ , and the apparent temperature  $\Gamma(x)T \propto \Gamma(x)^{1/2}$ . The apparent temperature of the fast shell is not much larger than that of the cork, any expansion of the shell further reduces its temperature, and its energy content is much smaller than that of the main cork. An inverse Compton contribution is also found to be much less energetic than other components (§ 5.2). Thus, we expect the fast shell to have little effect on the spectrum as well.

### 3.2. X-Ray Flash at the First Shock Emergence

We now consider the X-ray emission from the cork break-out. We assume that the cork expands at its speed of

sound at the cork break-out time,  $c_s \simeq c/\sqrt{3} = 0.58c$  in the relativistic case. This is the sound speed for a radiation-dominated gas, rarefaction fronts typically expanding at the speed of sound. As discussed above, at cork break-out the shock is at least mildly relativistic in the cases of interest here, so we use this limit from now on. For simplicity we replace the flattened cork (width =  $0.4\theta r <$  diameter =  $2\theta r$ ) with a sphere, and denote its radius by  $\Delta_0 = 2\theta r/3$ , which has the same volume. (The spherical expansion description in the comoving frame is a rough but convenient approximation, which becomes increasingly justifiable as the cork expands beyond one  $e$ -folding of its original dimensions at the same speed in all directions.) The cork's radius increases (in its comoving frame) as  $\Delta = \Delta_0 + c_s t$ . We therefore define the expansion factor

$$x \equiv 1 + c_s t/\Delta_0, \quad (7)$$

so that  $\Delta = \Delta_0 x$ ,  $\rho = \rho_0 x^{-3}$ ,  $T_r = T_{r,0} x^{-1}$ , and  $\tau_T = \tau_{T,0} x^{-2}$ . Subscripts 0 denote values at cork break-out time. Since the optical depth is very large, photons diffuse out of a thin skin depth at the edge of the cork. The width of the skin-depth layer out of which photons have escaped is  $\ell_{\text{diff}} \simeq (ct\Delta/3\tau_T)^{1/2}$ , where  $\Delta/\tau_T$  is the photon mean free path. We therefore have  $\ell_{\text{diff}}/\Delta \simeq (ct/3\Delta\tau_T)^{1/2} = (x/\tau_{T,0})^{1/2} (t/t_0)^{1/2}$ , where  $t_0 \equiv 3\Delta_0/c$ . The amount of energy radiated up to time  $t$  is

$$E_{\text{rad}} \simeq 4\pi\Delta^3 \frac{\ell_{\text{diff}}}{\Delta} aT^4 = \frac{3E_0}{\sqrt{\tau_{T,0}}} \left(\frac{t}{xt_0}\right)^{1/2}, \quad (8)$$

and hence the comoving luminosity is

$$L_{\text{rad}} \simeq \frac{3E_0}{2t_0\sqrt{\tau_{T,0}}} x^{-3/2} \left(\frac{t}{t_0}\right)^{-1/2}. \quad (9)$$

For times  $t \ll t_{\text{exp}} \equiv \Delta_0/c_s = (c/3c_s)t_0$ , the expansion is not important,  $x \simeq 1$ , hence  $L \propto t^{-1/2}$  and  $T_r \simeq T_{r,0}$ . At later times,  $x \gg 1$ ,  $L \propto t^{-2}$ , and  $T_r \propto t^{-1}$ . We note that the speed of sound in the shocked jet plasma is always (even for  $\beta_h \ll 1$ ) relativistic, so that the rarefaction wave crosses the shocked jet plasma much faster than it crosses the shocked stellar plasma. Since the internal energy stored in the shocked jet and stellar plasma are similar (from the momentum and energy conservation across the shock implied by the shock jump conditions), the expansion of the shocked jet plasma will accelerate the expansion of the shocked stellar plasma to a velocity larger by a factor of  $\sim \sqrt{2}$ . Thus, for arbitrary  $\beta_h$ , whether subrelativistic or relativistic, we can approximate  $t_{\text{exp}} \approx t_0/2\beta_h$ . The total energy radiated is thus

$$E_{\text{tot}} \simeq \frac{3E_0}{\sqrt{2}\beta_h\tau_{T,0}}. \quad (10)$$

One should keep in mind the potential limitations of the one-dimensional approximation used here, since in two-dimensional numerical calculations (e.g., Aloy et al. 2000; Zhang et al. 2002) the emergence of the reverse shock and rarefaction wave indicates the formation of a conical shape due to lateral expansion. For the parameters we used here, the one-dimensional approximation provides a useful description as long as the jet has not moved beyond much beyond  $\sim R_*\theta$ .

For a point on the source-observer line of sight, the characteristic break-out timescale  $t_{\text{exp}}$  is shortened to

$t_{\text{exp}}^{\text{obs}} = t_{\text{exp}}/2\Gamma_h = \Delta_0/2\Gamma_h c_s \approx 0.4\theta r/2\Gamma_h c_s$ . The angular smearing of the light curve occurs on a timescale  $dt_{\text{ang}}^{\text{obs}} \simeq \theta^2 r/2c$ , for which  $dt_{\text{ang}}^{\text{obs}}/t_{\text{exp}}^{\text{obs}} = 5\Gamma_h \theta c_s/2c < 5\theta\Gamma_h/2\sqrt{3}$ . Since  $\theta \ll 1$  and  $\Gamma_h$  is at most a few, we have  $dt_{\text{ang}}^{\text{obs}}/t_{\text{exp}}^{\text{obs}} \ll 1$ , and at a distance  $d$  the flux  $f \sim L/d^2$  of the observed pulse shape follows equation (9):  $f \propto t^{-1/2}$  for  $t < t_{\text{exp}}^{\text{obs}}$ ,

$$t_{\text{exp}}^{\text{obs}} = \begin{cases} 2.2L_{52}^{-1/4}\theta_{-1}r_{12.5}^{3/2}\rho_{-7}^{1/4} \text{ s}, & \text{H}, \\ 1.4 \times 10^{-1}L_{52}^{-1/4}\theta_{-1}r_{11}^{3/2}\rho_{-3}^{1/4} \text{ s}, & \text{He}, \\ 2.4 \times 10^{-2}L_{52}^{-1/4}\theta_{-1}r_{10}^{3/2}\rho_0^{1/4} \text{ s}, & \text{CO}, \end{cases} \quad (11)$$

and  $f \propto t^{-2}$  at later times (here  $d$  is distance of the source). The flux  $f_0$  (ergs  $\text{cm}^{-2} \text{s}^{-1}$ ) at  $t = t_{\text{exp}}^{\text{obs}}$  is approximately given by  $f_0 = \Gamma_h [3E_0/(2\tau_{\Gamma,s})^{1/2}]/(2t_{\text{exp}}^{\text{obs}})\pi(d/\Gamma_h)^2$  in the relativistic approximation,

$$f_0 = \begin{cases} 2.2 \times 10^{-9}L_{52}^{11/8}\theta_{-1}^{3/2}/r_{12.5}^{5/4}\rho_{-7}^{7/8}d_{28}^2, & \text{H}, \\ 4.9 \times 10^{-11}L_{52}^{11/8}\theta_{-1}^{3/2}/r_{11}^{5/4}\rho_{-3}^{7/8}d_{28}^2, & \text{He}, \\ 2.1 \times 10^{-12}L_{52}^{11/8}\theta_{-1}^{3/2}/r_{10}^{5/4}\rho_0^{7/8}d_{28}^2, & \text{CO}. \end{cases} \quad (12)$$

The rise time of the pulse, and hence the time at which the flux peaks, is

$$t_{\text{peak}}^{\text{obs}} \approx dt_{\text{ang}}^{\text{obs}} \approx \theta^2 r/2c = \begin{cases} 5.2 \times 10^{-1}\theta_{-1}^2 r_{12.5} \text{ s}, & \text{H}, \\ 1.7 \times 10^{-2}\theta_{-1}^2 r_{11} \text{ s}, & \text{He}, \\ 1.7 \times 10^{-3}\theta_{-1}^2 r_{10} \text{ s}, & \text{CO}, \end{cases} \quad (13)$$

and the peak flux (ergs  $\text{cm}^{-2} \text{s}^{-1}$ ) is

$$f_{\text{peak}} = \begin{cases} 4.4 \times 10^{-9}L_{52}^{5/4}\theta_{-1}/r_{12.5}\rho_{-7}^{3/4}, & \text{H}, \\ 1.4 \times 10^{-10}L_{52}^{5/4}\theta_{-1}/r_{11}\rho_{-3}^{3/4}, & \text{He}, \\ 7.4 \times 10^{-12}L_{52}^{5/4}\theta_{-1}/r_{10}\rho_0^{3/4}, & \text{CO}. \end{cases} \quad (14)$$

#### 4. CORK DYNAMICS FOLLOWING BREAK-OUT

At the time  $t = t_{\text{exp}}$  in the frame moving with Lorentz factor  $\Gamma_h$ , the rarefaction wave arrives at the backward shock decelerating the jet; the pressure behind this shock drops, and it can no longer decelerate the fast jet plasma. A new system of forward-backward shocks is formed, which propagates into the expanding cork plasma (see Fig. 1 for a schematic description). As the second forward shock breaks through the expanding cork, a second X-ray flash is produced. We consider the cork dynamics following the jet emergence in the relativistic limit, an approximation that is increasingly well satisfied.

##### 4.1. Second Shock

In the original frame of the shocked cork, moving with  $\Gamma_h$ , the shocked plasma expands, following the penetration of the rarefaction wave, with velocity comparable to the speed of sound,  $\approx c/\sqrt{3}$ . Adding (relativistically) this velocity to  $\Gamma_h$ , we find that the cork expands, in the source frame, with  $\Gamma'_h \approx (\sqrt{3}/2 + 1/\sqrt{2})\Gamma_h = 2\Gamma_h$ . Because of the expansion, the proper density of the expanding cork drops as  $\rho = \rho_0 x^{-3} = 4\Gamma_h \rho x^{-3}$ . Let us denote by  $\Gamma_{h2}$  the Lorentz factor (in the source frame) to which the rarefied cork plasma is

accelerated by the second shock driven by the jet. As the cork density decreases with time, the second shock accelerates. Balancing the pressure behind the new forward shock,  $3P_{h2} = 4(\Gamma_{h2}/2\Gamma'_h)^2 4\Gamma_h \rho x^{-3} c^2 = 4\Gamma_{h2}^2 \rho c^2 / 4\Gamma_h x^3$  (assuming the shock is relativistic), with the pressure behind the new backward shock,  $3P_r = 4(\Gamma_j/2\Gamma_{h2})^2 n_j m_p c^2$ , we find that  $\Gamma_{h2}$  is given by an expression similar to that determining  $\Gamma_h$ , with  $\rho$  replaced by  $\rho/4\Gamma_h x^3$ . Using equation (2) we therefore find

$$\frac{\Gamma_{h2}}{\Gamma_h} = (4\Gamma_h x^3)^{1/4}. \quad (15)$$

Note that if we had assumed that the new forward shock driven into the cork is not relativistic, pressure balance gives  $\beta_{h2} = x^{3/2}\Gamma_h^{1/2}/2$  for the shock velocity (in the frame where cork plasma is at rest), which implies that the shock is indeed relativistic.

In the frame moving with  $\Gamma_h$ , the forward shock Lorentz factor is  $\Gamma_s = \sqrt{2}\Gamma_{h2}/2\Gamma_h = (\Gamma_h x^3)^{1/4}$ . The shock breaks through the cork at time  $t$  for which the distance it travels, given by  $\int_{t_{\text{exp}}}^t dt(1 - 1/2\Gamma_s^2)c$ , equals the thickness of the expanded cork,  $x(t)\Delta_0$ . For  $\Gamma_h \rightarrow \infty$ ,  $\Gamma_s \rightarrow \infty$ , and second shock break-out occurs when  $x\Delta_0 = c(t - t_{\text{exp}}) = \sqrt{3}\Delta_0(x - 2)$ , i.e., for  $x = 2\sqrt{3}/(\sqrt{3} - 1) = 4.7$ . For finite  $\Gamma_h$ , crossing occurs at larger  $x$ , e.g., at  $x = 5$  for  $\Gamma_h = 4$ . We therefore adopt  $x = 5$  for the crossing time. Note that in this estimate we have assumed that  $\Gamma_{h2}$  is given by equation (15) throughout the second crossing. However, the cork is composed of shocked stellar plasma and shocked jet plasma. Equation (15) holds for propagation through the shocked stellar plasma, while shock propagation in the shocked jet plasma is faster, because of its lower density. However, since the shock crossing time for  $\Gamma_h = 4$  ( $x = 5$ ) is close to that obtained for  $\Gamma_s \rightarrow \infty$ , we neglect the small correction implied for the crossing time.

Following the second shock crossing, the new (proper) thickness of the shocked cork plasma is  $\Delta_2 \approx x\Delta_0/[4(\Gamma_{h2}/2\Gamma'_h)] = (x_c/4\Gamma_h)^{1/4}\Delta_0$ , where  $x_c \approx 5$  is the value of the expansion factor at shock break-out. The resulting second X-ray flash properties are estimated in § 5, following the same reasoning of § 3. We here give only the estimates for the dynamical cork parameters following the second crossing,

$$\frac{t_{\text{exp2}}}{t_{\text{exp}}} = \frac{\Delta_2}{\Delta_0} = \left(\frac{x_c}{4\Gamma_h}\right)^{1/4} \quad (16)$$

and

$$t_{\text{exp2}}^{\text{obs}} \equiv \frac{t_{\text{exp2}}}{2\Gamma_{h2}} = \frac{t_{\text{exp}}^{\text{obs}}}{2\sqrt{x_c}\Gamma_h} = \begin{cases} 4 \times 10^{-1}L_{52}^{-3/8}\theta_{-1}r_{12.5}^{7/4}\rho_{-7}^{3/8} \text{ s}, & \text{H}, \\ 3 \times 10^{-2}L_{52}^{-3/8}\theta_{-1}r_{11}^{7/4}\rho_{-3}^{3/8} \text{ s}, & \text{He}, \\ 8 \times 10^{-3}L_{52}^{-3/8}\theta_{-1}r_{10}^{7/4}\rho_0^{3/8} \text{ s}, & \text{CO}. \end{cases} \quad (17)$$

The proper thickness  $\Delta_2$  given by equation (16) is determined by the difference between the propagation speed of the (second) shock and the speed of the fluid behind the shock. This thickness, which is essentially the product of the speed difference and the shock life time, therefore grows with shock life time. The proper thickness saturates, i.e., ceases to increase, when the mass flux across the shock

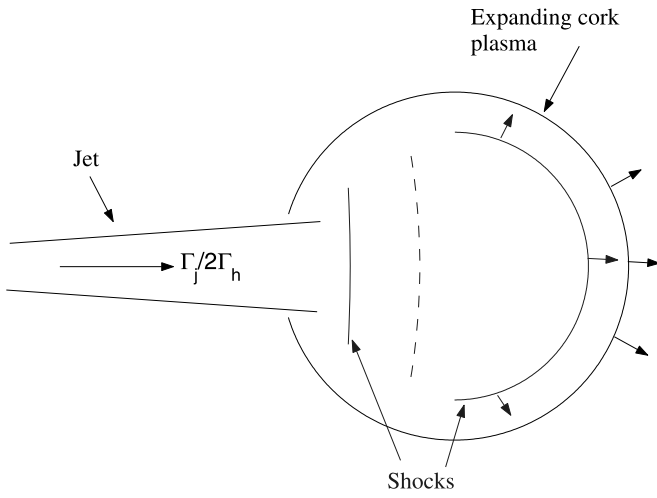


FIG. 2.—Schematic description of the flow during second shock propagation through the cork, as seen in the “isotropic cork frame” moving with  $\Gamma_h$ . [See the electronic edition of the *Journal* for a color version of this figure.]

equals the tangential mass flux (which is proportional to the thickness). In § 2, we have determined the proper thickness  $\Delta_0$  of the shocked cork plasma by balancing the two mass fluxes. Using the same argument here would have given  $\Delta_2 = \Delta_0$ . However, equation (16) gives  $\Delta_2 < \Delta_0$ , which implies that  $\Delta_2$  does not reach its asymptotic value during shock crossing.

Plasma expansion in the frame moving with  $\Gamma_{h2}$  is not isotropic. Following the first shock break-out, the plasma expands roughly isotropically in the frame moving with  $\Gamma_h$ , which we refer to in what follows as the “isotropic cork frame.” As the second shock propagates through this expanding plasma, the flow ahead of the shock is not uniform, and the geometry of the shock front is influenced by the shape of fluid streamlines ahead of the shock; the shock will no longer propagate radially in the source frame. This situation is schematically described in Figure 2. Since the Lorentz factor of the second shock, with respect to the fluid ahead of the shock, is not very large (see eq. [15]), we expect a large modification of the shock front geometry due to the nonuniform flow ahead of the shock. Assuming uniform pressure behind the shock implies uniform velocity of the shock front with respect to the fluid velocity ahead of the shock, i.e., radial shock expansion in the isotropic cork frame (moving with  $\Gamma_h$ ), where the preshock fluid expands isotropically. Following the second shock crossing, therefore, the shocked cork plasma fills, in the isotropic cork frame, a semispherical shell of proper thickness  $\Delta_2$ . This shell expands radially in the isotropic cork frame, with a Lorentz factor  $\Gamma_{h2}/2\Gamma_h$ . The fluid propagating along the jet axis propagates in the source frame with Lorentz factor  $\Gamma_{h2}$ , and expands over an observed expansion time given by equation (17).

#### 4.2. Third Shock

Following the second shock break-out, a second rarefaction wave propagates into the newly shocked cork, following which a third shock crosses the rarefied cork. We denote by  $\Gamma_{h3}$  the Lorentz factor in the source frame to which the rarefied cork plasma along the jet axis is accelerated by the

third shock. Here too, we expect the third shock to propagate radially, with Lorentz factor  $\Gamma_{h3}/2\Gamma_h$ , in the isotropic cork frame. We again define the expansion factor as  $x \equiv 1 + c_s t/\Delta_2$ , where  $t$  is the proper time, measured in the fluid rest frame from second shock break-out. Time  $\tilde{t}$  measured in the isotropic cork frame is related to the proper time through  $\tilde{t} = (\Gamma_{h2}/2\Gamma_h)t$ . The radius of the expanding shell in the isotropic cork frame at the second shock break-out is  $R \approx x_c c_s t_{\text{exp}} = x_c \Delta_0 \approx 2\theta r$ . This radius grows with time to  $R + \tilde{t}c \approx R + (\Gamma_h x_c^3)^{1/4} c \tilde{t}/\sqrt{2} = R[1 + \sqrt{3}/2(\Gamma_h/x_c)^{1/4} \tilde{t}/t_{\text{exp}}] = R[1 + (\sqrt{3}/2)\tilde{t}/t_{\text{exp}2}] \approx xR$ . Thus, the proper density of the expanding cork is  $\rho = \rho_1 x^{-3} = 4(\Gamma_{h2}/2\Gamma_h')^4 4\Gamma_h \rho (xx_c)^{-3} = 4\Gamma_{h2} \rho (xx_c)^{-3}$ . Balancing again the pressure behind the new forward shock,  $3P_{h3} = 4(\Gamma_{h3}/2\Gamma_h')^2 4\Gamma_{h2} \rho (xx_c)^{-3} c^2 = 4\Gamma_{h3}^2 \rho c^2 / 4\Gamma_{h2} (xx_c)^3$  (assuming a relativistic shock), with the pressure behind the new backward shock,  $3P_r = 4(\Gamma_j/2\Gamma_{h3})^2 n_j m_p c^2$ , we find that  $\Gamma_{h3}$  is given by an expression similar to that determining  $\Gamma_h$ , with  $\rho$  replaced by  $\rho/4\Gamma_{h2} (xx_c)^3$ . Using equation (2) we therefore find

$$\frac{\Gamma_{h3}}{\Gamma_h} = (4\Gamma_{h2} x_c^3 x^3)^{1/4} = 2^{5/8} x_c^{15/16} x^{3/4} \Gamma_h^{5/16}. \quad (18)$$

If we had assumed that the new forward shock is not relativistic, pressure balance would give  $\beta_{h3} = 0.5x_c^{3/8} x^{3/2} \Gamma_h^{1/8}$ , which implies that the shock is relativistic. Arguments similar to those presented above imply that the third shock crossing also occurs at  $x = x_c \approx 5$ . At the end of the third shock crossing we therefore have

$$\frac{t_{\text{exp}3}}{t_{\text{exp}}} = \frac{\Delta_3}{\Delta_0} = \left(\frac{x_c}{4\Gamma_h}\right)^{5/16} \quad (19)$$

and

$$t_{\text{exp}3}^{\text{obs}} \equiv \frac{t_{\text{exp}3}}{2\Gamma_{h3}} = \frac{t_{\text{exp}}^{\text{obs}}}{x_c^{11/8} (4\Gamma_h)^{5/8}} = \begin{cases} 7.5 \times 10^{-2} L_{52}^{-13/32} \theta_{-1} r_{12.5}^{29/16} \rho_{-7}^{13/32} \text{ s}, & \text{H}, \\ 7.0 \times 10^{-3} L_{52}^{-13/32} \theta_{-1} r_{11}^{29/16} \rho_{-3}^{13/32} \text{ s}, & \text{He}, \\ 1.7 \times 10^{-3} L_{52}^{-13/32} \theta_{-1} r_{10}^{29/16} \rho_0^{13/32} \text{ s}, & \text{CO}. \end{cases} \quad (20)$$

Finally, we note that at the end of the third shock crossing, the radius of the expanded cork, in the isotropic cork frame, is  $x_c R = x_c^2 \Delta_0$ , and the distance  $\delta r$  propagated by the cork along the jet axis is comparable to the stellar radius,  $\delta r \approx c\Gamma_{h2} x_c t_{\text{exp}2} \approx \sqrt{3} x_c^2 \Gamma_h \Delta_0 \approx \Gamma_h \theta_{-1} r$ .

Following the third rarefaction wave, the plasma is accelerated to  $\Gamma_{h3}' \approx 2\Gamma_{h3} \approx 50\Gamma_h^{21/16}$ , for which  $\Gamma_j/2\Gamma_{h3}' \approx \Gamma_j/100\Gamma_h^{21/16}$ . Thus, following the third shock crossing, the remnants of cork plasma in the jet path are accelerated to a high Lorentz factor. A strong fourth shock wave will be driven by the jet into this plasma only for  $\Gamma_j \gg 100$ .

## 5. X-RAY AND $\gamma$ -RAY PULSES FROM THE SECOND AND THIRD SHOCKS

### 5.1. Thermal Pulses

The thermal emission following the second and third shock crossings can be estimated using arguments similar to those of § 3. The energy density in the shocked cork plasma is proportional to  $L/r^2 \Gamma_{hi}^2$ , where subscripts  $i = 2, 3$  stand for second and third shock crossings, respectively. Thus,

$T_2 = T_r(\Gamma_{h2}/\Gamma_h)^{-1/2}$  and  $T_3 = T_r(\Gamma_{h3}/\Gamma_h)^{-1/2}$ , where  $T_r$  is given by equation (5). Using equations (15) and (18) we obtain for the temperature of the observed pulses

$$\Gamma_{h2}T_2 = (4\Gamma_h)^{1/8}x_c^{3/8}\Gamma_hT_r = \begin{cases} 6.2L_{52}^{13/32}/r_{12.5}^{13/16}\rho_{-7}^{5/32} \text{ keV}, & \text{H}, \\ 2.3 \times 10^1 L_{52}^{13/32}/r_{11}^{13/16}\rho_{-3}^{5/32} \text{ keV}, & \text{He}, \\ 5.1 \times 10^1 L_{52}^{13/32}/r_{10}^{13/16}\rho_0^{5/32} \text{ keV}, & \text{CO}; \end{cases} \quad (21)$$

$$\Gamma_{h3}T_3 = 2^{5/16}x_c^{27/32}\Gamma_h^{5/32}\Gamma_hT_r = \begin{cases} 1.4 \times 10^1 L_{52}^{53/128}/r_{12.5}^{53/64}\rho_{-7}^{21/128} \text{ keV}, & \text{H}, \\ 5.2 \times 10^1 L_{52}^{53/128}/r_{11}^{53/64}\rho_{-3}^{21/128} \text{ keV}, & \text{He}, \\ 1.1 \times 10^2 L_{52}^{53/128}/r_{10}^{53/64}\rho_0^{21/128} \text{ keV}, & \text{CO}. \end{cases} \quad (22)$$

Radiation emitted following the second shock crossing arrives at a distant observer lying along the jet axis from a cone around the jet axis of opening angle  $1/(\Gamma_{h2}/2\Gamma_h) = 2\Gamma_h/\Gamma_{h2}$  in the isotropic cork frame, where the shell radius is  $R = x_c\Delta_0$ . The angular time spread of the pulse is therefore given by  $dt_{\text{ang}2}^{\text{obs}} = (2\Gamma_h/\Gamma_{h2})^2 R/2(2\Gamma_h)c = \Gamma_h x_c \Delta_0 / \Gamma_{h2}^2 c$ . Comparing this time to the observed expansion time,  $t_{\text{exp}2}^{\text{obs}} = \sqrt{3}\Delta_2/2\Gamma_{h2}c = \sqrt{3}x_c\Gamma_h\Delta_0/2\Gamma_{h2}^2c$ , we find  $dt_{\text{ang}2}^{\text{obs}}/t_{\text{exp}2}^{\text{obs}} = 2/\sqrt{3} \approx 1$ . Thus, the second pulse is ‘‘smeared’’ over a duration  $dt_{\text{ang}2}^{\text{obs}}$ . Note that, had we assumed radial expansion in the source frame, the angular time spread would have been  $r/2\Gamma_{h2}^2c = (r/2x_c\Gamma_h\Delta_0)dt_{\text{ang}2}^{\text{obs}} \approx (2.5/\Gamma_h\theta_{-1})dt_{\text{ang}2}^{\text{obs}}$ . Thus, the resulting pulse duration is not sensitive to the detailed geometry of the shock front.

The proper energy in the cork plasma following the second shock crossing is  $E_2 = 2\pi R^2\Delta_2(aT_2^4) = 2\pi(x_c\Delta_0)^2(\Gamma_h x_c\Delta_0/\Gamma_{h2})a(\Gamma_{h2}/\Gamma_h)^{-2}T_r^4 = 2\pi\Delta_0^3(\Gamma_h x_c/\Gamma_{h2})^3 aT_r^4 \approx 0.3(\Gamma_h x_c/\Gamma_{h2})^3 E_0$ . Since the optical depth following the first crossing is reduced,  $\tau_{T,s2} = x_c^{-2}\tau_{T,s}$ , the flux of the second pulse (ergs  $\text{cm}^{-2} \text{s}^{-1}$ ) is  $f_2 \approx \Gamma_{h2}(3E_2/\sqrt{2\tau_{T,s2}})/2t_{\text{exp}2}^{\text{obs}}\pi(d/\Gamma_h^2) \approx 0.3x_c^3 f_0$ ,

$$f_2 \approx 0.3x_c^3 f_0 = \begin{cases} 8.6 \times 10^{-8} L_{52}^{11/8}\theta_{-1}^{3/2}/r_{12.5}^{5/4}\rho_{-7}^{7/8}, & \text{H}, \\ 6 \times 10^{-10} L_{52}^{11/8}\theta_{-1}^{3/2}/r_{11}^{5/4}\rho_{-3}^{7/8}, & \text{He}, \\ 1.1 \times 10^{-11} L_{52}^{11/8}\theta_{-1}^{3/2}/r_{10}^{5/4}\rho_0^{7/8}, & \text{CO}. \end{cases} \quad (23)$$

The duration of this pulse is given by equation (17).

Radiation emitted following the third shock crossing arrives at a distant observer lying along the jet axis from a cone around the jet axis of opening angle  $1/(\Gamma_{h3}/2\Gamma_h) = 2\Gamma_h/\Gamma_{h3}$  in the isotropic cork frame, where the shell radius is  $R = x_c^2\Delta_0$ . The angular time spread of the pulse is therefore given by  $dt_{\text{ang}3}^{\text{obs}} = (2\Gamma_h/\Gamma_{h3})^2 R/2(2\Gamma_h)c = \Gamma_h x_c^2 \Delta_0 / \Gamma_{h3}^2 c$ . Comparing this time to the observed expansion time,  $t_{\text{exp}3}^{\text{obs}} = \sqrt{3}\Delta_3/2\Gamma_{h3}c = \sqrt{3}x_c^2\Gamma_h\Delta_0/2\Gamma_{h3}^2c$ , we find  $dt_{\text{ang}3}^{\text{obs}}/t_{\text{exp}3}^{\text{obs}} = 2/\sqrt{3} \approx 1$ . Thus, the third pulse is ‘‘smeared’’ over a duration  $dt_{\text{ang}3}^{\text{obs}}$ . If we had we assumed radial expansion in the source frame, the angular time spread would have been  $r/2\Gamma_{h3}^2c = (r/2x_c^2\Gamma_h\Delta_0)dt_{\text{ang}3}^{\text{obs}} \approx (2.5/x_c\Gamma_h\theta_{-1})dt_{\text{ang}3}^{\text{obs}}$ . Thus, the resulting pulse duration is again not sensitive to the detailed geometry of the shock front.

The proper energy in the cork plasma following the third shock crossing is  $E_3 = 2\pi R^2\Delta_3(aT_3^4) = 2\pi(x_c^2\Delta_0)^2(\Gamma_h x_c^2\Delta_0/\Gamma_{h3})a(\Gamma_{h3}/\Gamma_h)^{-2}T_r^4 = 2\pi\Delta_0^3(\Gamma_h x_c^2/\Gamma_{h3})^3 aT_r^4 \approx 0.3(\Gamma_h x_c^2/\Gamma_{h3})^3 E_0$ . Since the optical depth following the third crossing is reduced,  $\tau_{T,s3} = x_c^4\tau_{T,s}$ , the flux (ergs  $\text{cm}^{-2} \text{s}^{-1}$ ) of the third pulse is  $f_3 \approx \Gamma_{h3}(3E_3/\sqrt{2\tau_{T,s3}})/2t_{\text{exp}3}^{\text{obs}}\pi(d/\Gamma_h^2) \approx 0.3x_c^6 f_0$ ,

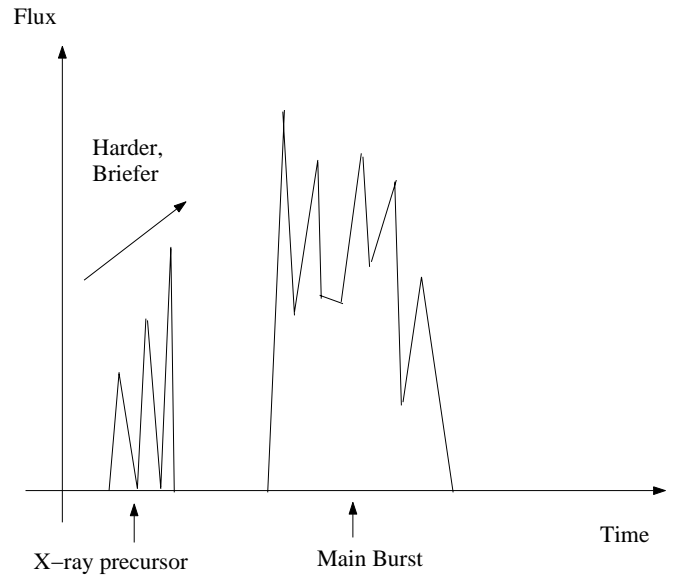


FIG. 3.—X-ray precursors of increasing flux and hardness and decreasing duration, resulting from successive shocks and rarefaction fronts moving across the cork of stellar material ejected by the GRB jet.

$\Gamma_{h3})^3 E_0$ . Since the optical depth following the third crossing is reduced,  $\tau_{T,s3} = x_c^4\tau_{T,s}$ , the flux (ergs  $\text{cm}^{-2} \text{s}^{-1}$ ) of the third pulse is  $f_3 \approx \Gamma_{h3}(3E_3/\sqrt{2\tau_{T,s3}})/2t_{\text{exp}3}^{\text{obs}}\pi(d/\Gamma_h^2) \approx 0.3x_c^6 f_0$ ,

$$f_3 \approx 0.3x_c^6 f_0 = \begin{cases} 1.1 \times 10^{-5} L_{52}^{11/8}\theta_{-1}^{3/2}/r_{12.5}^{5/4}\rho_{-7}^{7/8}, & \text{H}, \\ 7.7 \times 10^{-8} L_{52}^{11/8}\theta_{-1}^{3/2}/r_{11}^{5/4}\rho_{-3}^{7/8}, & \text{He}, \\ 1.4 \times 10^{-9} L_{52}^{11/8}\theta_{-1}^{3/2}/r_{10}^{5/4}\rho_0^{7/8}, & \text{CO}. \end{cases} \quad (24)$$

The X-ray pulses from the three shocks are schematically shown in Figure 3, appearing as precursors to the main burst emission.

## 5.2. Nonthermal Emission

As the shock approaches the shell edge, where the optical depth ahead of the shock drops to  $\sim 1$ , the radiation will escape and the shock will no longer be radiation dominated. It will most likely become collisionless. Waxman & Loeb (2001) have shown that, for a mildly relativistic shock, the ratio of electromagnetic instability growth rate and ion-ion (Coulomb) collision rate is  $\nu_{\text{EM}}/\nu_{i,i} \approx 10^7\rho_{-10}^{1/2}$ . The density at the third shock crossing is smaller than the initial stellar density by a factor  $\sim x_c^{-6}$ . Thus, for all the progenitors considered here, we have  $\nu_{\text{EM}}/\nu_{i,i} \gg 1$ , and the shock is likely to become collisionless, rather than collisional, as it approaches the edge of the cork, where the optical depth becomes of order 1. If a fourth shock crossing takes place, i.e., if  $\Gamma_j \gg 100$ , the fourth shock will be collisionless as well. For the BSG progenitor, the optical depth of the cork shell during third shock crossing is reduced to  $\sim 10$ . In this case, therefore, a significant fraction of the internal energy of the cork may be emitted as radiation from electrons accelerated to a nonthermal distribution by the collisionless shock.

We estimate below the nonthermal emission from the third shock as it becomes collisionless. In order to derive an estimate that is (nearly) independent of the details of the

preceding cork shocks dynamics, we use the following line of arguments. The isotropic-equivalent mass of plasma shocked by the collisionless shock is  $M_{\text{CL}} \approx 4\pi(\Gamma_h\theta_{-1}r)^2 \tau m_p / \sigma_T$ , where we have taken  $r_{\text{CL}} = \Gamma_h\theta_{-1}r$  as the shock radius (due to expansion of the plasma during the third shock crossing; see § 4) and  $\tau \sim 1$  is the optical depth ahead of the shock at the point it becomes collisionless ( $\tau m_p / \sigma_T$  is the corresponding column density). We have shown that the Lorentz factors of the shocks, in the frame at which the plasma ahead of the shocks is at rest, are of the order of a few. Thus, the isotropic-equivalent thermal energy generated by the collisionless shock is

$$E_{\text{CL}} \approx \Gamma_j \Gamma_i M_{\text{CL}} c^2 = \begin{cases} 7.7 \times 10^{50} \tau \Gamma_i \Gamma_{j,2.5} L_{52}^{1/2} \theta_{-1}^2 r_{12.5} \rho_{-7}^{-1/2} \text{ ergs}, & \text{H}, \\ 2.6 \times 10^{47} \tau \Gamma_i \Gamma_{j,2.5} L_{52}^{1/2} \theta_{-1}^2 r_{11} \rho_{-3}^{-1/2} \text{ ergs}, & \text{He}, \\ 8.6 \times 10^{44} \tau \Gamma_i \Gamma_{j,2.5} L_{52}^{1/2} \theta_{-1}^2 r_{10} \rho_0^{-1/2} \text{ ergs}, & \text{CO}, \end{cases} \quad (25)$$

where  $\Gamma_i \sim$  a few is the collisionless shock Lorentz factor (in the plasma frame). We have shown in § 4 that the proper thickness of the shocked cork shell following each shock passage is close to  $\Delta_0$ . The proper energy density behind the collisionless shock is therefore  $u_{\text{CL}} \approx (E_{\text{CL}}/\Gamma_j)/4\pi r_{\text{CL}}^2 (\Delta_0 \tau / \tau_{\text{CL}})$ , where  $\tau_{\text{CL}} \sim 10$  is the total optical depth of the shell at the stage where the collisionless shock is formed. Assuming that a fraction  $\xi_e$  ( $\xi_B$ ) of the thermal energy is carried by accelerated electrons (magnetic field), the characteristic frequency of synchrotron photons emitted by the electrons, accelerated to a characteristic Lorentz factor  $\gamma_e \approx \xi_e \Gamma_i$  ( $m_p/m_e$ ), is

$$h\nu_{\text{syn}} \approx \begin{cases} 7.9 \Gamma_i^{5/2} \xi_e^2 \sqrt{\tau_{\text{CL}} \xi_B} \Gamma_{j,2.5} \theta_{-1}^{-1/2} r_{12.5}^{-1/2} \text{ MeV}, & \text{H}, \\ 4.3 \times 10^1 \Gamma_i^{5/2} \xi_e^2 \sqrt{\tau_{\text{CL}} \xi_B} \Gamma_{j,2.5} \theta_{-1}^{-1/2} r_{11}^{-1/2} \text{ MeV}, & \text{He}, \\ 1.4 \times 10^2 \Gamma_i^{5/2} \xi_e^2 \sqrt{\tau_{\text{CL}} \xi_B} \Gamma_{j,2.5} \theta_{-1}^{-1/2} r_{10}^{-1/2} \text{ MeV}, & \text{CO}. \end{cases} \quad (26)$$

Thus, the third thermal (hard) X-ray pulse is accompanied by a nonthermal MeV gamma-ray pulse, with similar energy flux and duration.

An inverse Compton (IC) component is also expected, due to the thermal X-ray photons emitted from the cork that are upscattered by the fast jet,  $\Gamma_j \sim 10^2$ , as it emerges from the cork (Ramirez-Ruiz et al. 2002). The fluence of this IC component is significantly lower than the value estimated in the above reference, which was based on a simplified treatment assuming that all the thermal X-ray photons in the cork are upscattered by the relativistic jet. However, as shown in § 3.2, only a fraction  $\tau_{\text{T},0}^{-1/2} \ll 1$  of the thermal X-ray photons escape the cork and are available for upscattering (see eq. [10]); the value of  $\tau_{\text{T},0}^{-1/2}$  ranges from  $10^{-2}$  for the BSG progenitor to  $10^{-4}$  for the CO progenitor (see eq. [4]). Also, as shown in § 4, the fast jet emerges from the cork only after third shock crossing, at a time (measured in the star's frame)  $\approx \Gamma_{h2} x_c t_{\text{exp}2} \approx x_c^2 \Delta_0 / c$  after the first cork break-out. This time is much longer than the transverse light crossing time of the jet,  $\simeq \Delta_0 / c$ . Thus, most of the X-ray photons escape out of the jet's path prior to the emergence of the jet from the cork. We therefore conclude that the non-

thermal emission is dominated by the collisionless emission given by equations (25) and (26).

A second IC component may be produced if there is a  $\Gamma \sim 10\Gamma_1$  forerunner shell ejected ahead of the main cork, as discussed in § 3.1, from the upscattering of stellar photons by the forerunner. The number density of stellar photons drops as  $r^{-2}$ , so most of the fluence is produced by scattering of stellar photons near  $R_*$ , where  $R_*$  is the stellar radius. The (isotropic equivalent) energy of this IC component is  $\sim L_*(R_*/c)\Gamma^2 \sim 10^{37}\Gamma_1^2(L_*/L_\odot)$  ergs, where  $L_*$  is the stellar luminosity. This is much smaller than other high-energy components, such as equation (25).

## 6. DISCUSSION

We have shown that the emergence of a jet in a collapsar model of a GRB leads to a series of successive, increasingly shorter and harder thermal X-ray pulses. These are caused by successive cycles of shock waves and rarefaction waves reaching the outer and inner ends of the ‘‘cork’’ of stellar material being pushed ahead of the jet as it passes beyond the boundary of the stellar envelope. The Lorentz factor of the main bulk of the cork increases with each succeeding and increasingly relativistic shock that goes through it. A small fraction of the cork mass may be accelerated to larger Lorentz factors and run ahead of the cork, without significantly changing the development of the thermal pulses from the main bulk of the cork.

The expansion and acceleration of the main bulk of the cork lead to a decrease of the cork scattering optical depth, photon diffusion times, and expansion times in the observer frame for the successive shocks. As a result, the successive shocks have increasingly higher bolometric fluences and shorter durations, as well as harder peak photon energies. However, for observations in a fixed low-energy X-ray band, e.g., 2 keV, the specific fluence in  $\text{ergs cm}^{-2} \text{keV}^{-1}$  would be reduced by a Rayleigh-Jeans factor  $(E_{\text{obs}}/E_{\text{pk}})^2$  and would appear almost constant or slowly declining as the pulse number increases. On the other hand, in a hard X-ray detector, e.g.,  $\gtrsim 20$  keV, the successive pulses would show a steeply increasing fluence.

The results discussed here are based on analytical one-dimensional calculations in the relativistic limit. As argued in §§ 2 and 3, the approximations inherent in such an analytical treatment are reasonable for the range of parameters considered, but the flows considered are quite complex, and definitive results must await confirmation from more accurate numerical simulations. Current two-dimensional relativistic collapsar jet simulations (e.g., Aloy et al. 2000; Zhang et al. 2002) do not so far have the dynamic range and resolution necessary to distinguish multiple shocks and rarefaction waves upon emergence of the jet, but provide valuable information about the overall jet dynamics. The approximate analytical treatment presented here fulfill in the meantime an exploratory role, and provide insights for both future numerical and observational developments.

The temporal structure discussed provides distinct features, which should help to identify the phenomenon. We have argued (§ 2) that since jets are likely to accelerate to significantly relativistic velocities as they enter a much lower density H-envelope, the crossing time for a blue supergiant envelope may be only slightly longer than the core crossing time  $t_{\text{core}} \sim 30r_{11}$  s for He or CO dwarf stars. The initial rise time of the first pulse leading to the peak flux, given by the

angular smearing time, is  $t_{\text{pk}}^{\text{obs}} \sim (500, 20, 2)$  ms for a blue supergiant (H) star, a He star, and a CO star, occurring while the cork has not yet had time to expand. This is followed by a decay  $f \propto t^{-1/2}$  lasting an expansion time  $t_{\text{exp}}^{\text{obs}} \sim (2, 0.15, 0.025)$  s for the (H, He, Co) cases. Thereafter the flux drops as  $f \propto t^{-2}$ . The subsequent pulses have similar rise and decay times, given approximately by (increasingly shorter) observer-frame expansion times.

For stars of greater compactness (smaller radius) the characteristic bolometric fluxes, timescales, and fluences of each pulse are lower and shorter, while the peak temperatures are higher. The typical fluences from a Hubble distance  $d \sim 10^{28}$  cm range from  $\mathcal{F} \sim (5 \times 10^{-9}, 7 \times 10^{-12}, 5 \times 10^{-14})$  ergs  $\text{cm}^{-2}$  for the first pulse, to  $\mathcal{F} \sim (8 \times 10^{-7}, 5 \times 10^{-10}, 2 \times 10^{-12})$  ergs  $\text{cm}^{-2}$  for the third pulse, while the peak temperatures range from  $T_{\text{pk}}^{\text{obs}} \sim (1.6, 12, 50)$  keV for the first pulse, to  $T_{\text{pk}}^{\text{obs}} \sim (14, 52, 110)$  keV for the third pulse in (H, He, CO) stars, respectively.

After the third shock, the cork will have reached Lorentz factors comparable to the observationally inferred Lorentz factors in bursts ( $\Gamma \sim 100$ ). This shock may become collisionless, leading also to an additional nonthermal component of energy and duration comparable to the thermal third pulse, with characteristic photon energy  $E_{\gamma} \sim (8, 45, 140)$  MeV for (H, He, CO) stars.

With the fluences calculated here it is apparent that it would be easier to detect the X-ray pulses from extended GRB progenitors, such as blue supergiant (H) stars. The more compact progenitors (He or CO stars) would have lower fluences and be harder to detect, except for nearby objects, in which case they would be distinguishable from blue supergiant progenitors through their shorter peak durations and harder spectra. The characteristic precursor

thermal pulses, including the third thermal and nonthermal pulses described here, would precede the conventional MeV range emission by an appreciable timescale  $\sim t_{\text{exp}}^{\text{obs}} \sim 2.2 L_{52}^{-1/2} \theta_{-1}^{3/2} r_{12.5}^{3/2} \rho_{-7}^{1/4}$  s for blue supergiant (H) progenitors, or by shorter timescales  $\sim 0.15, 0.025$  s for He or CO progenitors.

It is conventionally assumed that the conditions for the usual successful GRB to occur is that the central engine powers the jet for timescales  $t_j$  longer than the stellar crossing time  $t_{\text{core}} \sim 30 r_{11}$  s. However, there may be cases in which the jet just breaks through the outer envelope of the star (whether it be a He, CO, or H BSG star), and does not live much longer afterward (e.g.,  $t_j \lesssim 30$  s). In this case, electromagnetic detectors will see only the thermal X-ray pulses and the hard nonthermal gamma-ray pulse ( $\gtrsim 10$  MeV; § 5.2), which last seconds or less. These would be a new class of objects, perhaps related to X-ray flash bursts and/or to short GRBs, especially if such events are more common and their distance is smaller.

The characteristic timescales as well as the ratios of the amplitudes and hardnesses of the pulses differ substantially, depending on the density and extent of the stellar envelope, which provides a potentially valuable diagnostic for pinning down the conditions in the preburst stellar progenitor. Instruments to be flown in the next several years, such as *Swift*, *GLAST*, *AGILE*, and others, should be able to detect such precursor signals in some bursts, and provide valuable clues concerning the GRB mechanism and their progenitors.

This research has been supported by NSF AST 00-98416, BSF 9800343, Universities Planning and Budget Committee, Israel, and NASA NAG5-9192.

#### REFERENCES

- Aloy, M., Müller, E., Ibañez, J., Martí, J., & MacFadyen, A. 2000, ApJ, 531, L119  
 Arnett, D. 1991, ApJ, 383, 295  
 Begelman, M., Blandford, R., & Rees, M. J. 1984, Rev. Mod. Phys., 56, 255  
 Frail, D. A., et al. 2001, ApJ, 562, L55  
 MacFadyen, A., Woosley, S., & Heger, A. 2001, ApJ, 550, 410  
 Martí, J., Müller, E., Font, J., Ibañez, J., & Marquina, A. 1997, ApJ, 479, 151  
 Matzner, C. D. 2002, MNRAS, submitted (astro-ph/0203085)  
 Matzner, C. D., & McKee, C. F. 1999, ApJ, 510, 379  
 Mészáros, P. 2002, ARA&A, 40, 137  
 Mészáros, P., & Rees, M. J. 2001, ApJ, 556, L37  
 Mészáros, P., & Waxman, E. 2001, Phys. Rev. Lett., 87, 171102  
 Paczyński, B. 1998, ApJ, 494, L45  
 Ramirez-Ruiz, E., McFadyen, A., & Lazzati, D. 2002, MNRAS, 331, 197  
 Sari, R., Waxman, E., & Shvarts, D. 2000, ApJS, 127, 475  
 Shigeyama, T., & Nomoto, K. 1990, ApJ, 360, 242  
 Waxman, E., & Loeb, A. 2001, Phys. Rev. Lett., 87, 071101  
 Woosley, S. E. 1993, ApJ, 405, 273  
 Woosley, S. E., Eastman, R. G., & Schmidt, B. P. 1999, ApJ, 516, 788  
 Woosley, S., Langer, N., & Weaver, T. 1993, ApJ, 411, 823  
 Zhang, W., Woosley, S., & McFadyen, A. 2002, ApJ, submitted (astro-ph/0207436)